


Long-Term Fatigue Damage Sensitivity to Wave Directionality in Extra Large Monopile Foundations

Journal Title
XX(X):1-??
©The Author(s) 2017
Reprints and permission:
sagepub.co.uk/journalsPermissions.nav
DOI: 10.1177/ToBeAssigned
www.sagepub.com/


Jan-Tore H. Horn ^{1,2}, Jørgen R. Krokstad ² and Jørgen Amdahl ^{1,2}

Abstract

The fatigue damage sensitivity to wave directionality on large-diameter monopile foundations for use in the offshore wind turbine industry is investigated. A frequency domain approach with the Dirlik method is used for a fatigue damage estimate and evaluate the effect of wave spreading and swell separation compared to a total sea representation. 30 years of hindcast data from the Dogger Bank area is used to evaluate the long-term impact. Furthermore, a computationally efficient time domain model of a 10 MW offshore wind turbine is used to compare with the frequency domain results. Results show that benefits in terms of structural fatigue can be obtained with directional considerations.

Keywords

Directionality, Fatigue, Hydrodynamics, Long-term statistics, Offshore environment, Offshore wind turbines, Swell

Introduction

The monopile foundation has proven to be the most cost-efficient solution in the offshore wind turbine industry due to its simple construction. As the rotor diameters and generator capacities are increasing to reduce the cost of energy, there is a need for large-diameter monopiles for up to 30-40 meters water depth. A consequence of the increasing submerged volume of the support structure is a higher sensitivity to wave loads for both FLS and ULS design considerations. This is in contrast to jacket foundations, where the wave load contribution is found to be significantly less than the wind loads¹, being less sensitive to wave directionality and swell separation.

The overall goal for the offshore wind industry is to reduce the levelized cost of energy (LCoE) to be able to compete with non-renewable sources of electricity. There are many ways to achieve cost reduction, but the focus here is on design conservatism. Being a low-margin industry, both investment and operational costs play an important role in the profitability of an offshore wind farm. Hence, accurate analysis models for use in the structural design are important. The topic of this paper is important for substructure designs that are driven by wave loads. Previous studies have been performed on hydrodynamic load models for monopile foundations, and the outcome has been compared with industry standards^{2,3} and model tests⁴. These account for typical sea states for both FLS and ULS design, and findings include the importance of wave diffraction and non-linear load effects such as ringing⁵. In general, the purpose is to de-risk monopile support structures for larger turbines and greater water depths.

A previous study has been performed⁶ to find reduction factors for fatigue damage for various types of wave directionality. Although the wave environment is somewhat idealized, the result indicates a large potential for reduced conservatism and correspond well with the short-term fatigue factors (FF) obtained in the present work. It has previously

been demonstrated how a directional distribution can be used for probabilistic analyses⁷, and the effects on selection and determination of the extreme design wave criteria^{8,9}. These investigations have shown that care must be taken in a design process when using directional distribution of environmental conditions and directional bins. One might end up with a less reliable structure than intended for ULS design considerations. For FLS design, it will here be demonstrated how a directional consideration can increase the structural reliability and to what extent the circumferential fatigue damage depends on load directionality.

In the present work, both a frequency- and a time domain model are implemented in order to qualitatively compare the effects of wave directionality with the different approaches. The frequency domain model is expected to be a good approximation when evaluating the FLS conditions where the contribution from non-linear wave loads and structural response can be neglected.

Model Description

The computational model used in this work is the onshore DTU 10 MW reference wind turbine¹⁰ mounted on an offshore monopile foundation. To keep the first natural period realistically low, the original tower is stiffened by increasing the thickness 20%. The turbine is located in 30 meters of water depth at Dogger Bank in the North Sea and 60 years of hindcast data are retrieved from the Norwegian

¹Centre for Autonomous Marine Operations and Systems (NTNU AMOS)

²Department of Marine Technology, Norwegian University of Science and Technology, Trondheim, Norway

Corresponding author:

Jan-Tore H. Horn, NTNU AMOS, Department of Marine Technology, Otto Nielsen veg 10, 7491 Trondheim, Norway.

Email: jan-tore.horn@ntnu.no

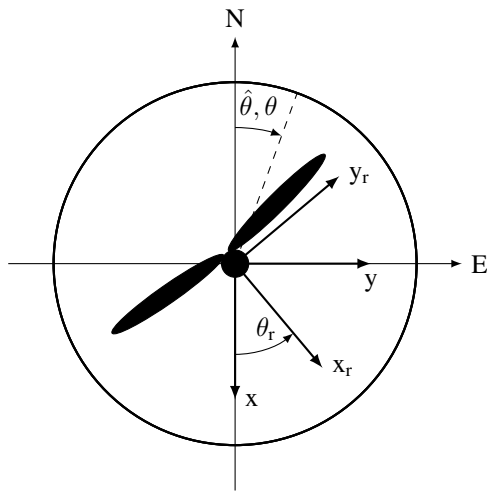


Figure 1. Directional definitions for environment (θ), monopile circumference ($\hat{\theta}$) and rotor plane (θ_r)

Meteorological Institute¹¹ for an approximate location. The monopile has a simplified design with a constant outer diameter from 42 meters below the mudline to the tower base at 10 meters above sea level (m.a.s.l.). The part from -10 to 10 m.a.s.l. is defined as the transition piece, which is stiffened by increasing the monopile thickness by 36%. Here, the monopile diameter and thickness are 8.0 and 0.11 meters, respectively, partly based on a preliminary design¹². The structural model is illustrated in Fig. 2 with all components manufactured in steel, with a 8% density increase in the transition piece and tower to account for secondary structures. As a result, the first and second natural period of the system are approximately 4.4 and 0.9 seconds. The numerical analyses are carried out with USFOS¹³, with a computationally efficient model. Beams are used for the monopile and tower in the FEM analysis, while the soil stiffness is modelled using an equivalent cantilever beam tuned to properly represent realistic eigenmodes³ and natural periods mentioned above. Wave loads are calculated by the Morison equation with correction for linear diffraction and a vertical stretching to the free surface.

This paper focuses on the effects of directionality on the environmental loads, it is therefore necessary to define the wind turbine operational conditions in relation to the north-east (NE) frame as well as the local frame (xy) and rotor-frame ($x_r y_r$). These definitions are illustrated in Fig. 1.

Environmental conditions

The environmental conditions used in simulations are obtained from the hindcast data. The most important parameters for description of the offshore environment are given in Tab. 1, while the remaining parameters can be found in Tab. 2. It is assumed that the wind speed at 100 m.a.s.l. is equal the wind speed at hub height, which is located at 119 m.a.s.l. Also, no corrections are made to the hindcast data with respect to local bathymetry. Except for parameters related to current, spreading and spectral peak shape, information is readily available. Scatter diagrams and joint contour plots can be found in the appendix for the simulated data.

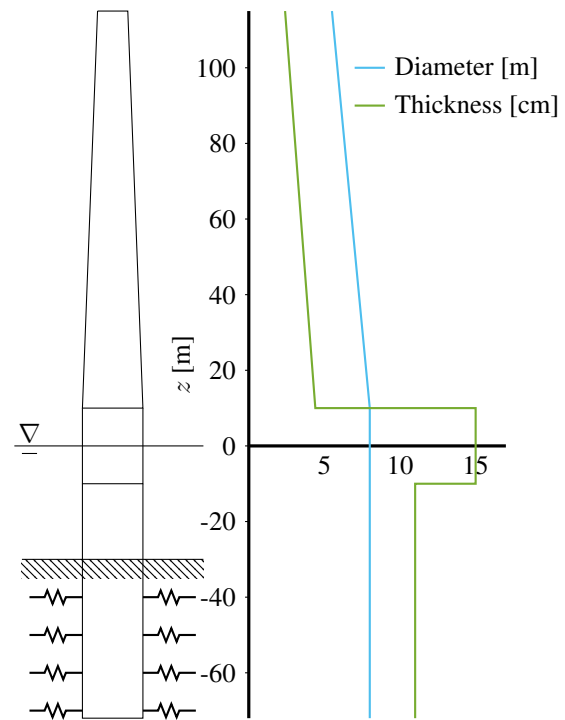


Figure 2. Structural dimensions of tower and monopile foundation

In Fig. 3, the circular probability density functions (PDF) of the some environmental parameters are presented. The most likely wind and wind sea direction is from the south-west, while swell is mostly coming from the northern North Sea. It is clear that the total sea distribution is significantly influenced by the swell component. To get an idea about the direction of the most energetic waves, the directional data is weighted by the significant wave heights squared. The result is shown in Fig. 4 and by the available information, it is expected that the wave-induced fatigue damage will be largest at north or south side of the foundation.

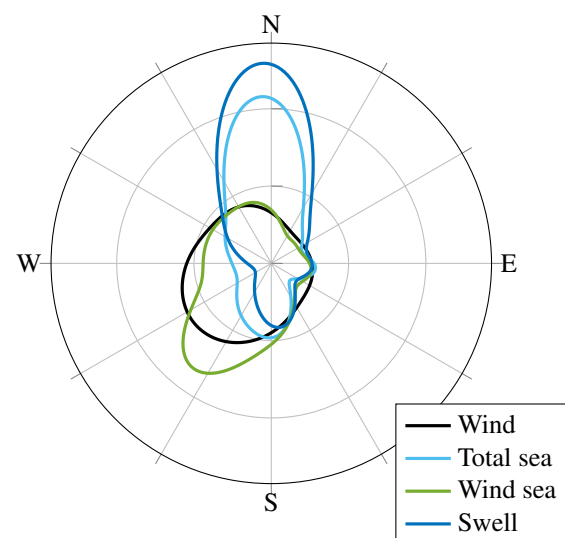


Figure 3. Directional marginal distributions of environmental parameters

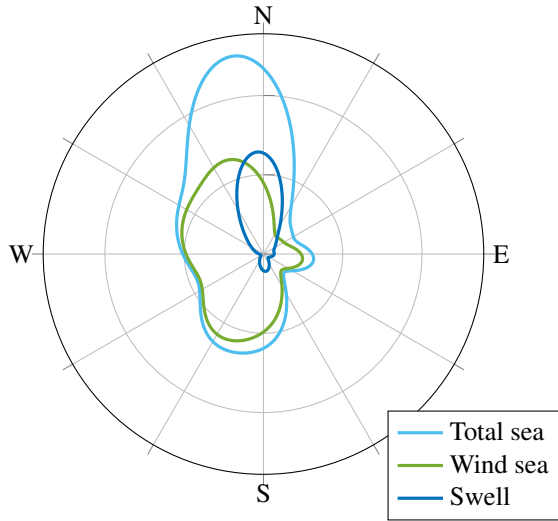


Figure 4. Directional marginal distributions of environmental parameters weighted with the square of the respective significant wave heights

Table 1. Primary parameters for description of environmental conditions

	Description	
Θ_u	Mean wind heading relative to N	[deg]
Θ	Mean total sea direction relative to N	[deg]
U	Mean wind speed at 100m.a.s.l.	[m/s]
H_S	Significant wave height for total sea	[m]
T_P	Peak period for total sea	[s]
γ	Peak shape parameter for total sea	[-]
h	Water depth	[m]

Table 2. Secondary parameters for description of environmental conditions

	Description	
Θ_w	Mean wind-sea direction relative to N	[deg]
Θ_s	Mean swell direction relative to N	[deg]
H_{S_w}	Significant wave height for wind sea	[m]
H_{S_s}	Significant wave height for swell	[m]
T_{P_w}	Peak period for wind sea	[s]
T_{P_s}	Peak period for swell	[s]
γ_w	Peak shape parameter for wind sea	[-]
γ_s	Peak shape parameter for swell	[-]
s	Spreading exponent for wind sea	[-]
X	Spreading parameter for swell	[-]
V_c	Current velocity	[m/s]
Θ_c	Current direction	[deg]

This work will present results from five different variations on wave directionality in addition to the long-term mean direction variation:

- Long-crested total sea (L)
- Short-crested total sea (S)
- Long-crested wind sea and long-crested swell (LL)
- Short-crested wind sea and long-crested swell (SL)
- Short-crested wind sea and short-crested swell (SS)

Availability

The availability of a wind turbine is defined as the proportion of the time it is capable of producing power.

The aerodynamic damping level of the turbine decreases dramatically when the turbine is not operating, which is an important parameter for fatigue estimation. This relation is becoming more important as the wind turbines are getting larger, meaning that the relative difference between operational and non-operational damping level is increasing. It has been reported that current offshore wind farms have an availability between 90 and 95%¹⁴, which is slightly less than land-based turbines. Final results are therefore presented using both 90 and 100% availability to find any impact on the fatigue damage using the different directional descriptions. To account for the fact that the unavailability may occur at any time during the total lifecycle, simulations with 0 and 100% availability are superimposed after weighting with the percentage of total availability. The fatigue damage is then found as:

$$D = D_{\text{unavail}} \cdot (1 - \alpha) + D_{\text{avail}} \cdot \alpha \quad (1)$$

where α is the availability fraction.

Directional wave spectrum

According to design standards¹⁵, the total wave spectrum can be modelled as a superposition of the wind sea and swell spectrum with their respective generalized spreading functions:

$$S_{\zeta\zeta}(\omega, \theta) = S_w(\omega)\Delta_w(\omega, \theta) + S_s(\omega)\Delta_s(\omega, \theta) \quad (2)$$

The JONSWAP spectrum is used for both wind sea and swell spectrum, and the peak shape parameters is a function of the significant wave height and peak period¹⁵. The spreading function for wind sea in infinite water depth is given as a \cos - $2s$ distribution¹⁶:

$$\Delta_w(\omega, \theta) = \frac{\Gamma[s(\omega) + 1]}{2\sqrt{\pi}\Gamma[s(\omega) + 1/2]} \cos^{2s(\omega)}\left(\frac{\theta - \Theta_w}{2}\right) \quad (3)$$

for a frequency dependent spreading exponent s . For practical purposes, the spreading exponent is often considered frequency independent, which in general is more conservative¹⁷. The established frequency dependent spreading functions are all based on wave measurements and are on the form:

$$s(\omega) = s_p \left(\frac{\omega}{\omega_p}\right)^\mu \quad (4)$$

as seen in e.g.^{18;19}. Observations have shown that the spreading exponent is decreasing for frequencies away from the peak frequency, and that it is in dependent on the wave age. For practical purposes, s is often regarded as a constant between 4 and 9¹⁵. Here a model described in Tucker²⁰ and implemented in Krokstad¹⁷ is used, where:

$$s_p = \begin{cases} 6.97 & \text{for } \omega < 1.05\omega_p \\ 9.77 & \text{for } \omega \geq 1.05\omega_p \end{cases} \quad (5)$$

and

$$\mu = \begin{cases} 4.06 & \text{for } \omega < 1.05\omega_p \\ -1.91 & \text{for } \omega \geq 1.05\omega_p \end{cases} \quad (6)$$

Further, the directional distribution of the swell component can be approximated by a Poisson distribution²¹, also assuming infinite water depth:

$$\Delta_s(\omega, \theta) = \frac{1}{2\pi} \frac{1 - X(\omega)^2}{1 - 2X(\omega) \cos(\theta - \Theta_s) + X(\omega)^2} \quad (7)$$

where

$$X(\omega) = X_p \left(\frac{\omega}{\omega_p} \right)^\nu \quad (8)$$

using $X_p = 0.9$ ²², and

$$\nu = \begin{cases} 2.21 & \text{for } \omega < \omega_p \\ -0.35 & \text{for } \omega \geq \omega_p \end{cases} \quad (9)$$

When the swell is modelled as long-crested, $\Delta_s = 1$ for $\theta = \Theta_s$ and zero elsewhere.

SN-curves

Fatigue damage at the mudline is calculated using SN-curves in both the frequency- and the time domain with the SN-curves given in Tab. 3²³. The predicted number of cycles until failure, N , is found with

$$\log N_n = \log K_n - \beta_n \log (\Delta\sigma(t/t_{\text{ref}})^{k_t} \cdot \text{SCF}) \quad (10)$$

for a given stress range $\Delta\sigma$ and material parameter β . Further, t is the cross section thickness, t_{ref} is the reference thickness and k_t is the thickness exponent. Here, $n = 1$ for a single-slope SN-curve and

$$n = \begin{cases} 1 & \text{for } \Delta\sigma \geq s_0 \\ 2 & \text{for } \Delta\sigma < s_0 \end{cases} \quad (11)$$

for two-slope SN-curves. For practical reasons, the single-slope SN-curves are used in frequency domain analyses, corresponding to elements without cathodic protection. The fatigue damage from the time domain simulations is estimated using rainflow counting and the Palmgren-Miner rule with the WAFO toolbox²⁴.

Table 3. Three different SN-curves

SN-curve	1	2	3
β_1	3	5	3
β_2	-	-	5
$\log K_1$	11.764	15.606	11.764
$\log K_2$	-	-	15.606
s_0 [MPa]	-	-	52.63
k_t	0.2	0.2	0.2
t_{ref} [mm]	25	25	25
SCF	1.0	1.0	1.0

Wind sea and swell compared to total sea

To facilitate comparisons between directionally dependent sea state realizations, the energy in the wave spectrum must be conserved. From the hindcast generated wind sea and swell components, the total significant wave height can be found as¹⁵:

$$H_S = \sqrt{H_{S_w}^2 + H_{S_s}^2} \quad (12)$$

The above equation for significant wave height compares very well to the hindcast data for total sea. However, finding the equivalent total sea peak period from the swell and wind sea components is not straightforward. Therefore, a typical design approach is performed; the simulated total sea is based purely on the hindcast data with default peak shape factor¹⁵. As a consequence, the total spectral energy may differ between the total sea spectrum and the spectrum based on both wind sea and swell.

Fatigue factor

The fatigue factor (FF) from simulations using directional spreading is calculated as:

$$\text{FF}_S = \frac{\max[D_S(\hat{\theta})]}{\max[D_L(\hat{\theta})]} \quad (13)$$

for all directions of evaluation in the vector $\hat{\theta}$ about the circumference of the foundation. The FF is an indication of how much the maximum circumferential fatigue damage has changed compared to analyses with long-crested total sea. A similar expression is used for all wave direction variations.

Frequency domain model

Mudline bending moment transfer function

Using the Morison equation as a basis, the linearized total complex force per unit length from an undisturbed wave field is given as:

$$\begin{aligned} f_x &= \zeta_a \rho \pi r^2 C_M a_x + \zeta_a^2 \rho r C_D |u_x| u_x \\ &\approx \zeta_a \left\{ \rho \pi r^2 C_M a_x + \rho r C_D \sqrt{\frac{8}{3\pi}} \sigma_u u_x \right\} \\ &= \zeta_a \cdot \bar{f}_x(\omega, \sigma_u) \end{aligned} \quad (14)$$

where r is the monopile radius and C_M is the mass coefficient corrected for diffraction and

$$u_x = -i\omega \frac{\cosh k(z+h)}{\sinh kh} \quad (15)$$

$$a_x = \omega^2 \frac{\cosh k(z+h)}{\sinh kh} \quad (16)$$

The drag coefficient is assumed to be constant equal to one, while the particle velocity standard deviation is found with:

$$\sigma_u^2(\theta) = \int_0^\infty \omega^2 S_{\zeta\zeta}(\omega, \theta) d\omega \quad (17)$$

Following the order of magnitude definition in Horn et al.³ and Faltinsen²⁵, and assuming a rigid body, one degree-of-freedom system with no radiation effects, the moment transfer function is obtained as:

$$\bar{M}_y(\omega) = \int_{-h}^0 \bar{f}_x \cdot (z+h) \cdot dz + O(\epsilon^2 \delta^2) \quad (18)$$

and the following relation is utilized:

$$\int_{-h}^0 (z+h) \cdot \frac{\cosh k(z+h)}{\sinh kh} dz = \frac{hk - \tanh \frac{hk}{2}}{k^2} \quad (19)$$

The resulting spectrum for the mudline bending moment can then be found as:

$$S_{MM}(\omega, \theta) = |\bar{M}_y(\omega)|^2 \cdot S_{\zeta\zeta}(\omega, \theta) \quad (20)$$

Dynamic amplification factor

An investigation on dynamic amplification of marine structures can be found in e.g. Horn et al.²⁶. Due to the linear response characteristics of a mass-dominated structure, it is sufficient to use the single harmonic dynamic amplification factor (DAF)²⁷:

$$DAF(\omega, \theta, U) = \frac{1}{\sqrt{(1 - \Omega^2)^2 + (2\zeta\Omega)^2}} \quad (21)$$

where $\Omega = \frac{\omega}{\omega_1}$ and ω_1 is the first natural period of the system, neglecting contribution from higher modes. Estimating the damping level is not straightforward, especially in irregular seas. In general, the damping level is found as:

$$\zeta = \zeta_a(\theta, U) + \zeta_s + \bar{\zeta} \quad (22)$$

for a structural damping level ζ_s , here equal to 0.5%, wind- and directionally dependent aerodynamic damping ζ_a presented later, and some additional damping $\bar{\zeta}$, which is here calibrated to approximately 5% to account for damping induced by hydrodynamic loads in an irregular sea. The modified bending moment spectrum is then:

$$S_{MM}(\omega, \theta, U) = |\bar{M}_y \cdot DAF|^2 \cdot S_{\zeta\zeta} \quad (23)$$

Circumferential fatigue damage distribution

The axial stress at a location $\hat{\theta}$ on a cylindrical beam element due to axial load and bending moments can be expressed in the time domain as:

$$\begin{aligned} s_z(\hat{\theta}) &= \frac{N}{A} - \frac{M_y \cdot r \cos \hat{\theta}}{I_A} - \frac{M_x \cdot r \sin \hat{\theta}}{I_A} \\ &= \frac{N}{A} - \sum_{\theta \in \theta} \frac{M_\theta \cdot r \cos(\hat{\theta} - \theta)}{I_A} \end{aligned} \quad (24)$$

for loads acting in directions contained in θ . Here, A is the cross sectional area, N is the axial force, I_A is the second area moment of the cross section and M_x , M_y and M_θ are the bending moments in x-, y- and θ -direction, respectively. Taking the variance yields:

$$\sigma_s^2(\hat{\theta}) = \sum_{\theta \in \theta} \sigma_s^2(\hat{\theta}|\theta) \quad (25)$$

where

$$\sigma_s^2(\hat{\theta}|\theta) = \frac{r^2}{I_A^2} \cdot \sigma_M^2(\theta) \cdot \cos^2(\hat{\theta} - \theta) \quad (26)$$

and the variance of the directionally dependent moments is found by integrating the response spectrum:

$$\sigma_M^2(\theta) = \int_0^\infty S_{MM}(\omega, \theta) d\omega \quad (27)$$

Dirlik method

The fatigue damage in the frequency domain is evaluated using the Dirlik method²⁸. At a circumferential location $\hat{\theta}$, the damage due to a load acting in direction θ is:

$$\begin{aligned} D^{DK}(\hat{\theta}|\theta) &= C \cdot \sigma_s^\beta(\hat{\theta}|\theta) \left[G_1 Q^\beta \Gamma(1 + \beta) \right. \\ &\quad \left. + \sqrt{2}^\beta \Gamma(1 + \frac{\beta}{2}) (G_2 |R|^\beta + G_3) \right] \end{aligned} \quad (28)$$

where $C = \nu_p \cdot T \cdot K^{-1} \cdot (t/t_{ref})^{\beta \cdot k_t} \cdot SCF^\beta$, and the G_1 , G_2 , G_3 , R and Q parameters read:^{28;29}

$$\begin{aligned} G_1 &= \frac{2(x_m - \alpha_2^2)}{1 + \alpha_2^2} & G_2 &= \frac{1 - \alpha_2 - G_1 + G_1^2}{1 - R} \\ G_3 &= 1 - G_1 - G_2 & R &= \frac{\alpha_2 - x_m - G_1^2}{1 - \alpha_2 - G_1 + G_1^2} \\ Q &= \frac{1.25(\alpha_2 - G_3 - G_2 R)}{G_1} \end{aligned} \quad (29)$$

Further, the α_2 , x_m and ν_p parameters are calculated as:

$$\begin{aligned} \alpha_2 &= \frac{m_2}{\sqrt{m_0 m_2}} & x_m &= \frac{m_1}{m_0} \left(\frac{m_2}{m_4} \right)^{\frac{1}{2}} \\ \nu_p &= \sqrt{\frac{m_4}{m_2}} \end{aligned} \quad (30)$$

by using the n^{th} spectral moment defined as:

$$m_n = \int_0^{2\pi} \int_0^\infty \omega^n S(\omega, \theta) d\omega d\theta \quad (31)$$

By integrating over the load directions for the sea state, a short-term fatigue damage is found as:

$$D_n^{DK}(\hat{\theta}) = \frac{1}{2\pi} \int_{-\pi}^\pi D^{DK}(\hat{\theta}|\theta) d\theta \quad (32)$$

Finally, the long-term fatigue damage is calculated by superposition over N individual sea states:

$$D^{DK}(\hat{\theta}) = \sum_{n=1}^N D_n^{DK}(\hat{\theta}) \quad (33)$$

Time domain model

Wave kinematics

The wave kinematics for time domain analysis are computed using the Matlab-based, in-house program WaveSim³. Wave loads to the first order are included, in addition to a vertical stretching of the first order kinematics to the linear free surface which introduces second order forcing terms³.

Aerodynamics

When using constant wind, assuming stationary conditions and neglecting rotor-induced loads, there is no need for a rotor or control system. Instead a constant force is applied to account for the structural displacements due to mean aerodynamic thrust given by:

$$F_a = \frac{1}{2} \rho_a \pi R^2 C_T(U) U^2 \quad (34)$$

where R is the rotor radius and the thrust coefficient is taken as:

$$C_T(U) = \begin{cases} 0.8 & \text{for } 4 \leq U < 11 \\ 39e^{-0.37U} + 0.13 & \text{for } 11 \leq U \leq 25 \\ 0.0 & \text{else} \end{cases} \quad (35)$$

Aerodynamic damping is accounted for using dashpot dampers at the tower top during simulations. The rotor-induced damping is dependent on both wind speed and

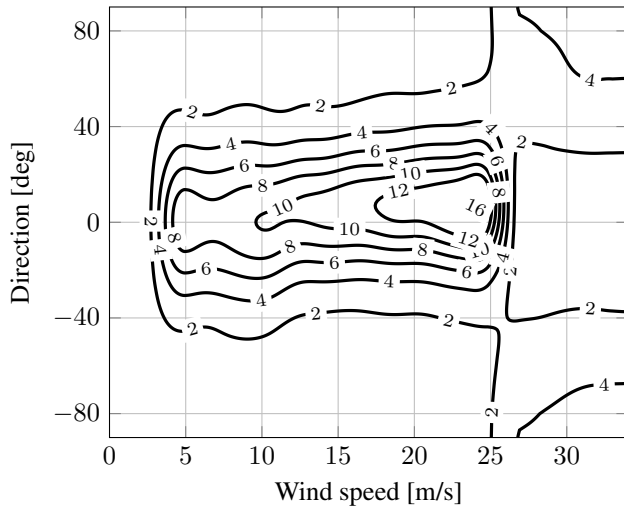


Figure 5. Aerodynamic damping coefficient ζ_a as a function of wind speed and vibration direction

vibrational direction. A complete model of the DTU 10 MW reference wind turbine¹⁰ is used to estimate the damping on the present foundation. The results are presented in Fig. 5, and it is seen that there is a significant level of aerodynamic damping in operational conditions for vibrational modes aligned with the wind direction. Interestingly, there is a significant difference in damping level for a tower top vibrational direction of -15 and 15 degrees for higher wind speeds. This is simply due to the clockwise rotation of the turbine when looking downwind, introducing a larger drag on the blade due to the relative velocity. Also, above the cut-out wind speed, when the rotor is idling with a blade pitch angle of 82 degrees, there is larger side-to-side than fore-aft damping. This indicates that the blades can contribute to the aerodynamic damping even in non-operational conditions. In the frequency domain, the wind and directionally dependent damping is found by interpolation, while the applied dashpot damping in time domain is the fore-aft and side-to-side damping ratios only. As a result, the damping in time domain will decrease proportionally with cosine, meaning that the damping coefficient will be over-predicted for small to intermediate wind-wave misalignment angles. The lower limit of aerodynamic damping is 1%.

Theoretical fatigue factors

In this section a theoretical fatigue damage reduction will be derived using a spectral method and narrow-banded response. Due to the non-linearity of separating the swell component from the fatigue damage expression, this is only done for long- and short-crested waves with the same wave spectrum and frequency independent spreading. First, the fatigue factor, FF, for a single sea state is derived in Eqn. (36). Here, the FF is evaluated in the same direction as the mean direction of the incoming waves, i.e. $\hat{\theta} = 0$ and $\bar{\theta} = 0$, where $\bar{\theta}$ is the mean direction. The closed-form solution in Eqn. (36) corresponds exactly to the wave kinematics factor (WKF) for long-crested waves¹⁵ reproduced in Eqn. (37), with the relationship $FF = WKF^\beta$. Some example values are given in Tab. 4 for the FF in a single sea-state. These values indicate that in a short-term perspective, a large reduction in

the fatigue damage can be expected when using short-crested sea, depending on the bandwidth of the directional spreading.

Table 4. Theoretical short-term fatigue factors for short-crested compared to long-crested waves using two SN-curves (SN) and three spreading exponents (s)

		s		
		4	6	9
SN	1	0.59	0.67	0.75
	2	0.41	0.52	0.62

$$FF = \frac{D_S}{D_L}(\hat{\theta} = 0 | \bar{\theta} = 0) = \frac{\sigma_{s,SC}^\beta}{\sigma_{s,LC}^\beta}(\hat{\theta} = 0 | \bar{\theta} = 0) \quad (36a)$$

$$= \frac{[\int_{-\pi}^{\pi} \sigma_{M,SC}^2(\theta) \cdot \cos^2(\theta) d\theta]^{\beta/2}}{\sigma_{M,LC}^\beta} \quad (36b)$$

$$= \left[\int_{-\pi}^{\pi} \Delta_w(\theta) \cdot \cos^2(\theta) d\theta \right]^{\beta/2} \quad (36c)$$

$$= \left[\frac{\Gamma(s+1)}{2\sqrt{\pi}\Gamma(s+1/2)} \int_{-\pi}^{\pi} \cos^{2s}\left(\frac{\theta}{2}\right) \cos^2(\theta) d\theta \right]^{\beta/2} \quad (36d)$$

$$= \left[\frac{\Gamma(s+1)}{\Gamma(s+1/2)} \cdot \frac{(s^2+s+1)\Gamma(s+1/2)}{\Gamma(s+3)} \right]^{\beta/2} \quad (36e)$$

$$= \left[\frac{s^2+s+1}{(s+1)(s+2)} \right]^{\beta/2} \quad (36f)$$

$$WKF = \sqrt{\frac{s^2+s+1}{(s+1)(s+2)}} \quad (37)$$

Now, the long-term FF will be derived under the assumption that the wave loads are uniformly distributed from all directions. Since the environmental loads are assumed to have the same severity in all directions, so will the fatigue damage. Hence, setting $\hat{\theta} = 0$ as the point of evaluation is sufficient. The fatigue factors for N uniformly distributed environmental conditions from north to south is then given as:

$$\frac{D_S}{D_L}(\hat{\theta} = 0) = \frac{\sum_{n=1}^N \sigma_{s,SC}^\beta(\bar{\theta}_n)}{\sum_{n=1}^N \sigma_{s,LC}^\beta(\bar{\theta}_n)} \quad (38a)$$

$$= \frac{\sum_{n=1}^N [\int_{-\pi}^{\pi} \Delta_w(\theta) \cdot \cos^2(\theta - \bar{\theta}_n) d\theta]^{\beta/2}}{\sum_{n=1}^N [\cos^2(\bar{\theta}_n)]^{\beta/2}} \quad (38b)$$

Here, no closed-form solution is available, but the FF has converged for $N > 20$. The numerically evaluated factors are found in Tab. 5, and as expected, the fatigue reduction is smaller in a long-term perspective compared to a single sea state. It is also seen that the FF is less dependent on

the wave spreading exponent. For offshore wind turbines, the fatigue damage is expected to have a significant contribution from high-cycle fatigue, meaning that the FFs for $\beta = 5$ may dominate the results when a quasi-static response assumption is valid. Hence, there is a potential for reducing the FLS design conservatism.

Table 5. Theoretical long-term fatigue factors for short-crested compared to long-crested waves for two SN-curves (SN) and three spreading exponents (s)

		s		
		4	6	9
SN	1	0.86	0.88	0.90
	2	0.60	0.66	0.73

From the fatigue factors in Tab. 5, one can show that use of the wave kinematics factor in Eqn. (37) is conservative for $\beta = 5$ and non-conservative for $\beta = 3$, meaning that the WKF should be applied with care in a long-term directionally dependent fatigue evaluation.

Long-term fatigue damage predictions

Results are presented for frequency domain analysis using the latest 30 years of raw data and time domain simulations with five years of data, or approximately 15,000 individual sea states. The computational efforts are very small in the frequency domain, but the time domain simulations through five years requires over 3,000 CPU-hours, even with a computationally efficient model with a real- to simulation time ratio of 18:1.

The complete multivariate results are found in the appendix, where the correlations between fatigue factors and environmental conditions are visualized.

Frequency domain analysis

Results from simulations with a constant spreading exponent are shown in the rosette in Fig. 6. The corresponding fatigue factors are found in Tab. 6, including fatigue factors when including frequency wave spreading. For the single slope SN-curve with $\beta = 3$ there is no change in the long-term fatigue damage using a short-crested formulation for the total sea. Theoretically a damage reduction of 10% is expected, but due to non-uniform directional environmental loads, the total maximum fatigue does not change significantly. This is true for both constant and frequency dependent spreading. When using a larger material exponent as in SN-curve 2, the effect of wave spreading is beneficial in terms of reduced fatigue damage. Explained by the increased importance of reduced loading and less impact from directional components away from the main propagation direction.

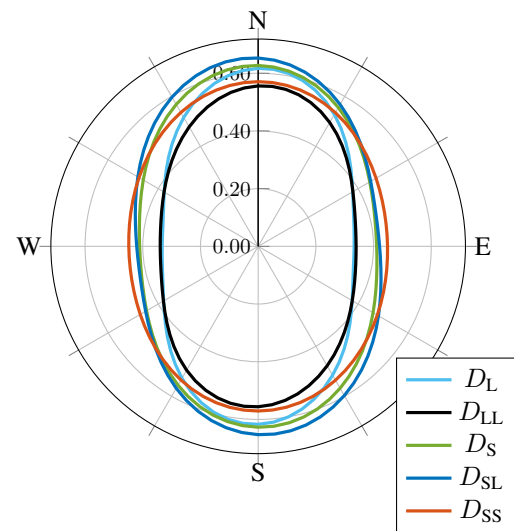
When swell is separated from the spectrum, meaning that the wind sea and swell spectrum are superimposed, there is a benefit in spread energy, but there is also a larger probability of significant misalignment angles between the swell- and wind direction. For swell significant wave height comparable to the wind sea wave height, this may excite low-damped vibrational modes. This effect is not captured completely in the frequency domain as the structure is assumed to be excited in-line with the individual wave components, while

in time domain such components may rather contribute to excitation of other low-damped directions. Significant reduced fatigue damage is observed, when the swell is modelled as short-crested. Now, more of the energy from the swell is propagating in directions affected by the aerodynamic damping, and hence reducing the response.

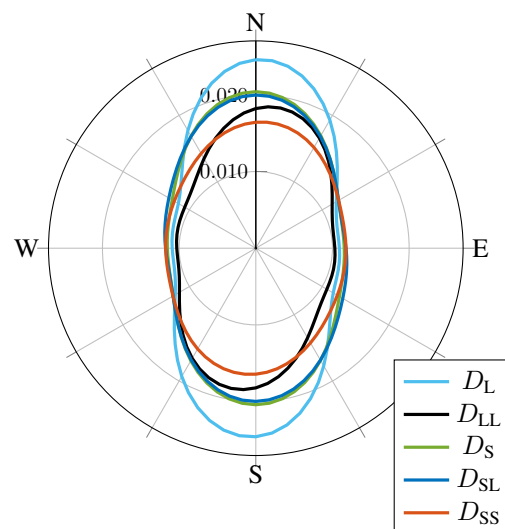
Table 6. Fatigue factors from frequency domain analyses with single-slope SN-curves (SN) and 100% availability. Normalized w.r.t. long-crested sea (L)

SN	Spreading							
	$s = 9$				$s(\omega)$			
	LL	S	SL	SS	LL	S	SL	SS
1	0.90	1.00	1.04	0.92	0.90	1.02	1.11	0.99
2	0.76	0.83	0.81	0.67	0.76	0.79	0.84	0.70

Total fatigue damage using 90% availability is presented in Fig. 7. The fatigue has increased by approximately 40-50% for SN-curve 2 by comparing Fig. 6b and 7b, stating the importance of including unavailability. Relative

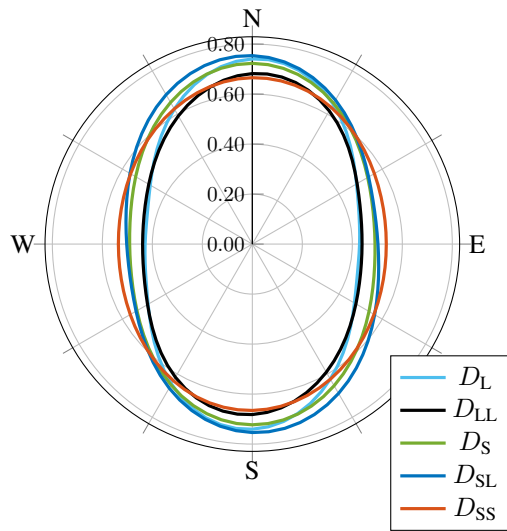


(a) SN-curve 1

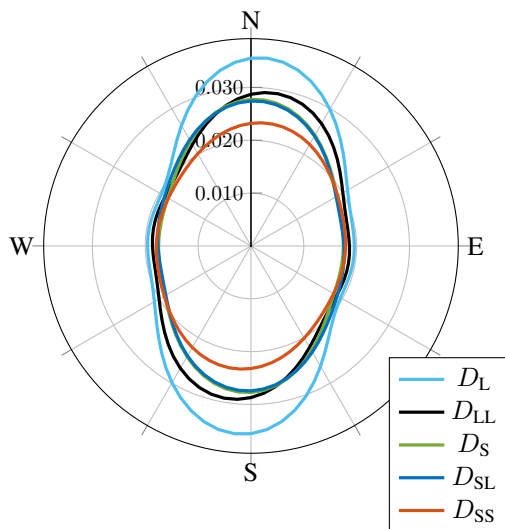


(b) SN-curve 2

Figure 6. 20-year circumferential fatigue damage at mudline using Dirlik method in the frequency domain and 20 years of data with spreading exponent $s = 9$.



(a) SN-curve 1



(b) SN-curve 2. S and SL configuration overlap.

Figure 7. 20-year circumferential fatigue damage at mudline using Dirlik method in the frequency domain and 20 years of data with 90% availability and spreading exponent $s = 9$

differences with respect to long-crested sea are found in Tab. 7 and show that spreading is increasingly important when considering availability, in terms of reducing the expected fatigue damage.

Table 7. Fatigue factors from frequency domain analyses with SN-curve 1, 90% availability and spreading exponent $s = 9$. Normalized w.r.t. long-crested sea (L)

SN	LL	S	SL	SS
1	0.92	0.97	1.02	0.89
2	0.82	0.77	0.76	0.65

Time domain analysis

Results from time domain analysis confirm qualitatively what was observed in frequency domain. Hence, the simple one degree-of-freedom frequency is a good indicator for variations in fatigue. The circumferential fatigue damage from time domain simulations is plotted in Fig. 8,

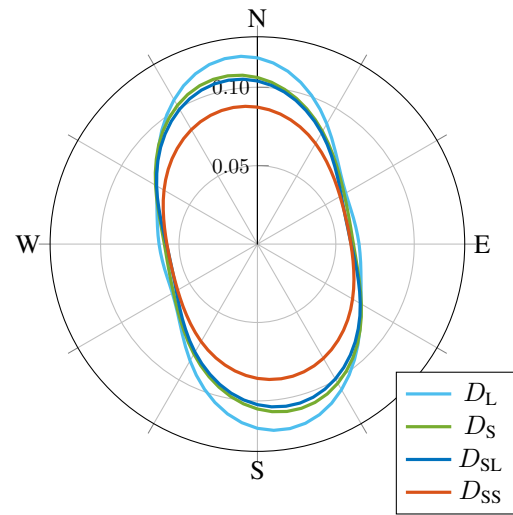


Figure 8. 20-year circumferential fatigue damage at mudline using dynamic time domain simulations and 5 years of data. SN-curve 3 and spreading exponent $s = 9$.

which shows a high degree of correlation with Fig. 6b indicating that the high-cycle part of the SN-curve is dominating the results. The corresponding fatigue factors are presented in Tab. 8, showing slight fatigue reductions, especially when modelling the swell as short-crested. Note that the circumferential distribution is shifted slightly counterclockwise, because the wind turbine model used in time domain simulations are only able to translate in one direction at the time, meaning that more wave components will excite lightly damped vibrational directions. Comparing with Fig. 3 and 4, the maximum fatigue occurs at the location excited by most wave energy, but has the largest probability of misaligned wind and waves.

Table 8. Fatigue factors from time domain analyses with bi-linear SN-curve and spreading exponent $s = 9$. Normalized w.r.t. long-crested sea (L)

	S	SL	SS
	0.90	0.88	0.74

Discussions and conclusions

It is concluded that the effects of wave spreading and swell separation on the long-term fatigue damage are somewhat smaller than initially expected. It may even result in lower fatigue life when a low-cycle SN-curve is used for members without corrosion protection. However, the more realistic high-cycle and bi-linear SN-curves show a fatigue damage reduction potential of up to 35%, which is of significance. From the current analyses, it is clear that any benefit from wave directionality on the structural fatigue damage is site dependent as the statistical correlation between wind and swell direction is an important parameter for dynamic amplification and rotor-induced damping. Therefore, any cost reductions related to less conservative environmental modelling for both FLS and ULS design must be performed with respect to the governing measurements or hindcast data. For the present case, a 35% increase in fatigue damage is equivalent to a thickness reduction of approximately 6% if

one assume that the dynamic behaviour of the system does not change and SN-curve 2 is used. As the cost of the foundation is directly related to the wall thickness of the monopile, it will contribute to lowering the levelized cost of energy. Of course, one needs to include the response due to turbulent wind when assessing the overall cost reduction.

It would be of interest to compare the presented results with a water depth dependent spreading function. Such a correction should account for the fact that incoming waves may develop a narrower spreading when propagating to shallower waters and introduce different frequency dependencies on the spreading exponent. This is especially important for extreme sea states, but to a lesser degree when fatigue is of primary interest. The spreading effect on fatigue damage is expected to have a significant effect when the turbine is idling above the cut-out wind speed of 25m/s as indicated in the scatter plots in the appendix. Therefore, the validity of spreading in extreme sea needs to be validated by on-site measurements.

For wind sea, the spectral peak period is the main contributor to response excitation, while the misalignment angle is more important for swell, whose direction is statistically independent of the wind and wind sea direction. When the turbine is operating, and aerodynamic damping is significant, both the swell direction and a peak period close to the natural period is important for fatigue damage through dynamic amplification. Introduction of unavailability is important for fatigue damage from the operational periods. When the turbine is in a non-operational condition, the fatigue reduction effect of directionality in all its presented forms are more evident.

In further work it is recommended to include the directional formulations presented in this paper in a fully coupled aero-servo-hydro-elastic simulation in order to quantify the overall effects when loads from turbulent wind are included.

Acknowledgements

This work has been carried out at the Centre for Autonomous Marine Operations and Systems (NTNU AMOS). The Norwegian Research Council is acknowledged as the main sponsor of NTNU AMOS. This work was supported by the Research Council of Norway through the Centres of Excellence funding scheme, Project number 223254 - NTNU AMOS. The authors would also like to thank the Norwegian Meteorological Institute for access to hindcast data.

References

- Dong W, Moan T and Gao Z. Long-term fatigue analysis of multi-planar tubular joints for jacket-type offshore wind turbine in time domain. *Engineering Structures* 2011; 33(6): 2002–2014. DOI:10.1016/j.engstruct.2011.02.037.
- Bachynski EE and Ormberg H. Hydrodynamic modeling of large-diameter bottom-fixed offshore wind turbines. In *Proceedings of the ASME 34th International Conference on Ocean, Offshore and Arctic Engineering*. St. Johns, Canada: ASME.
- Horn JTH, Krokstad JR and Amdahl J. Hydro-Elastic Contributions to Fatigue Damage on a Large Monopile. *Energy Procedia* 2016; .
- Fürst Frimann-Dahl J. Master thesis: Experimental Validation and Design Review of Wave Loads on Large-Diameter Monopiles. Technical report, Norwegian University of Science and Technology, 2015.
- Krokstad J, Stansberg C, Nestegaard A et al. A New Nonslender Ringing Load Approach Verified Against Experiments. *Journal of Offshore Mechanics and Arctic Engineering* 1998; 120(1): 20. DOI:10.1115/1.2829515.
- Vugts JH. Fatigue damage assessments and the influence of wave directionality. *Applied Ocean Research* 2005; 27(3): 173–185. DOI:10.1016/j.apor.2005.11.003.
- Mathisen J, Ronold KO and Sigurdsson G. Probabilistic Modelling for Reliability Analysis of Jackets. In *23rd International Conference on Offshore Mechanics and Arctic Engineering, Volume 2*. ASME. ISBN 0-7918-3744-0, pp. 231–239. DOI:10.1115/OMAE2004-51227.
- Sterndorff MJ and Sørensen JD. A Rational Procedure for Determination of Directional Individual Wave Heights. In *Proceedings of the 20th International Conference on Ocean, Offshore and Arctic Engineering - OMAE 2001*. Rio de Janeiro, Brazil: ASMA.
- Ewans K and Jonathan P. The Effect of Directionality on Northern North Sea Extreme Wave Design Criteria. *Journal of Offshore Mechanics and Arctic Engineering* 2008; 130(4): 041604. DOI:10.1115/1.2960859.
- Bak C, Zahle F, Bitsche R et al. Description of the DTU 10 MW Reference Wind Turbine. Technical report, DTU, 2013.
- Reistad M, Breivik Ø, Haakenstad H et al. A high-resolution hindcast of wind and waves for the North Sea, the Norwegian Sea, and the Barents Sea. *Journal of Geophysical Research: Oceans* 2011; 116(5): 1–18. DOI:10.1029/2010JC006402. [1111.0770](https://doi.org/10.1029/2010JC006402).
- Velarde J. Master thesis: Design of monopile foundations to support the DTU 10MW wind turbine. Technical report, Norwegian University of Science and Technology, 2016.
- USFOS. User Manual. Technical report, 2014. URL <http://www.usfos.no>.
- GL Garrad Hassan. A guide to UK offshore wind operations and maintenance. Technical report, 2013.
- DNV GL. RP-C205 Environmental conditions and environmental loads. Technical report, 2010.
- Simanesew A, Krogstad HE, Trulsen K et al. Development of frequency-dependent ocean wave directional distributions. *Applied Ocean Research* 2016; 59: 304–312. DOI:10.1016/j.apor.2016.06.011. URL <http://dx.doi.org/10.1016/j.apor.2016.06.011>.
- Krokstad JR. Sensitivity of Directional Spreading for Low-Frequency Motions in Short-Crested Waves. *Proceedings of the Fourth (1994) International Offshore and Polar Engineering Conference* 1994; III: 564–574.
- Mitsuyasu H, Tasai F, Suhara T et al. Observations of the directional spectrum of ocean waves using a coverleaf buoy, 1975. DOI:10.1175/1520-0485.
- Hasselmann DE, Dunckel M and Ewing JA. Directional Wave Spectra Observed during JONSWAP 1973. *Journal of Physical Oceanography* 1980; 10.
- Tucker MJ. *Waves in Ocean Engineering, Measurements, Analysis, Interpretation*. Ellis Horwood Limited, 1991.
- Krogstad HE, Barstow SF, Haug O et al. Directional distributions in wave spectra. In *Proceedings of the*

- International Symposium on Ocean Wave Measurement and Analysis*.
22. Bitner-Gregersen EM and Hagen Ø. Directional spreading in two-peak spectrum at the Norwegian continental shelf. In *Proceedings of the International Conference on Offshore Mechanics and Arctic Engineering*.
 23. DNV GL. RP-C203 Fatigue design of offshore steel structures. Technical Report April, 2005.
 24. WAFO-group. WAFO - A Matlab Toolbox for Analysis of Random Waves and Loads, 2000. URL <http://www.maths.lth.se/matstat/wafo/>.
 25. Faltinsen OM, Newman JN and Vinje T. Nonlinear wave loads on a slender vertical cylinder. *Journal of Fluid Mechanics* 1995; 289: 179. DOI:10.1017/S0022112095001297.
 26. Horn JTH, Amdahl J and Haver SK. Dynamic Amplification of Drag Dominated Structures in Irregular Seas. In *Proceedings of OCEANS'15 MTS/IEEE Washington Conference & Exhibition*. IEEE conference proceedings. ISBN 978-0-933957-43-5.
 27. ABS. Guidance Notes on Dynamic Analysis Procedure for Self-Elevating Drilling Units. Technical report, 2014.
 28. Dirlik T. *Application of Computers in Fatigue Analysis*. PhD Thesis, The University of Warwick, 1985.
 29. Mršnik M, Slavič J and Boltežar M. Frequency-domain methods for a vibration-fatigue-life estimation - Application to real data. *International Journal of Fatigue* 2013; 47: 8–17. DOI:10.1016/j.ijfatigue.2012.07.005.

Appendix

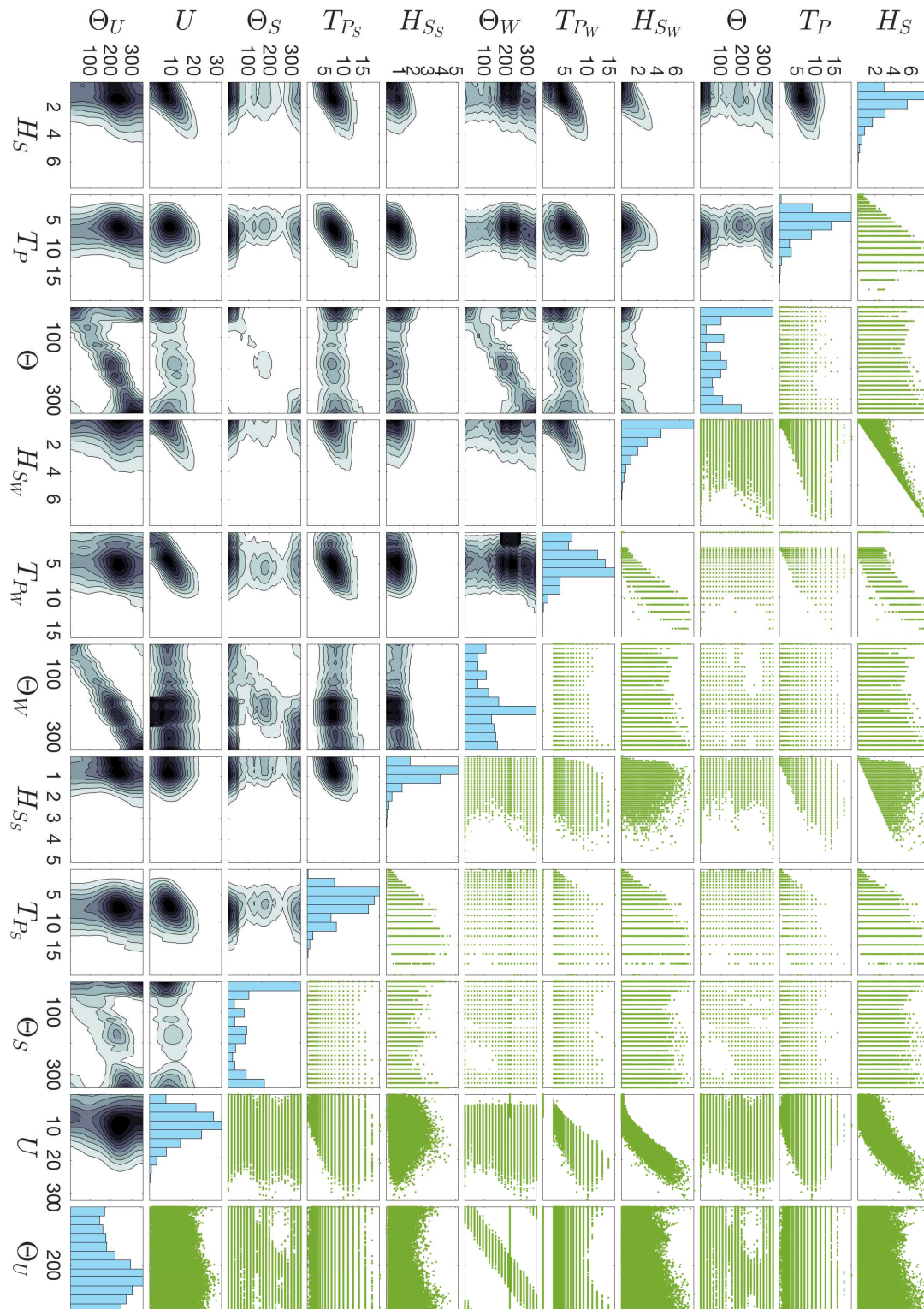


Figure 9. 30 years of unfiltered hindcast data at Dogger Bank with marginal histograms and qualitative joint contour plots

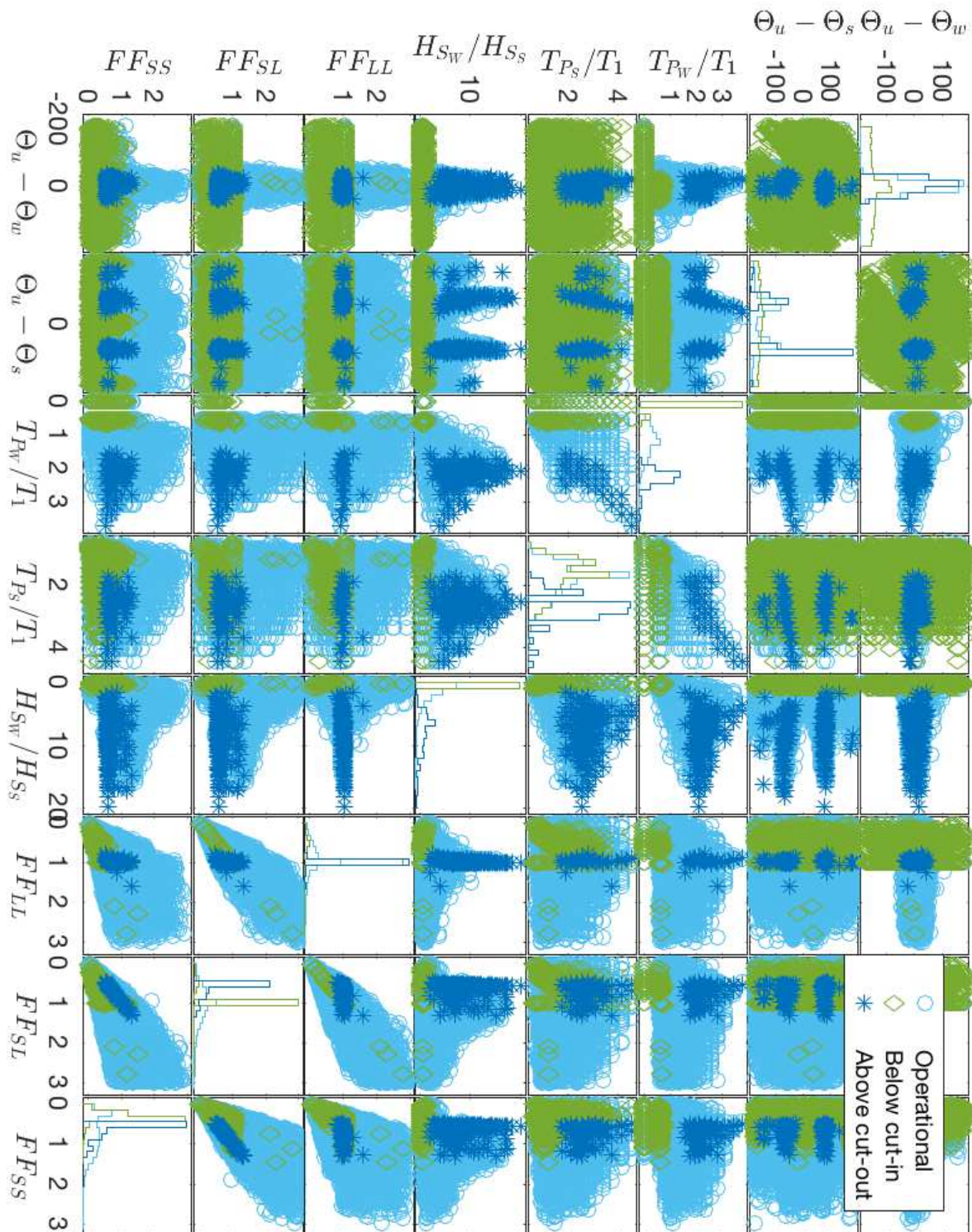


Figure 10. Correlations between environmental parameters and fatigue factors with 100% availability. T_1 is the first natural period.

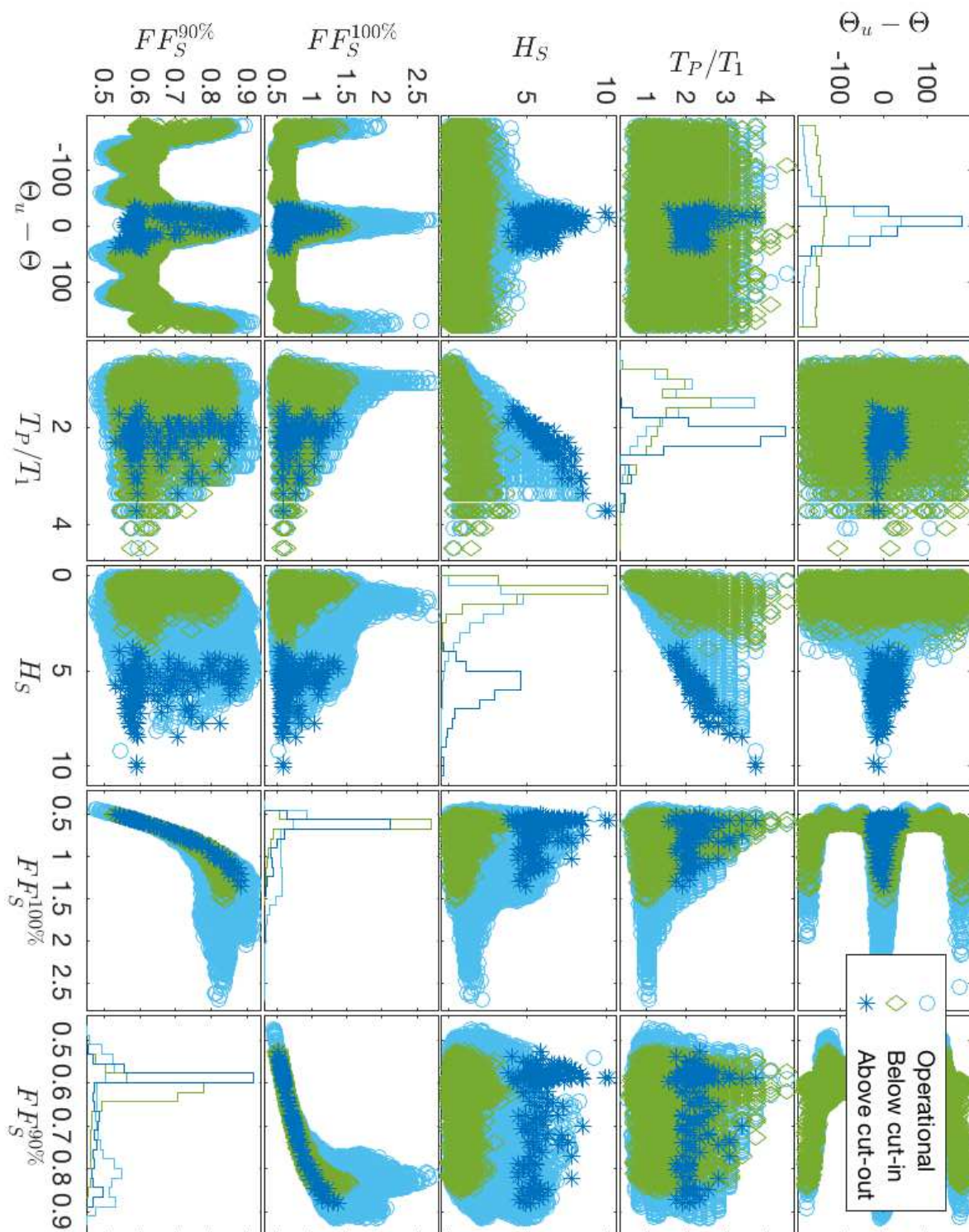


Figure 11. Correlations between environmental parameters and fatigue factors with 90% and 100% availability for short-crested total sea. T_1 is the first natural period.